Atomistic Underpinnings for Orientation Selection in Alloy Dendritic Growth

C. A. Becker,[1,*] D. Olmsted,[2] M. Asta,[3] J. J. Hoyt,[2] and S. M. Foiles[2]

[1]*Department of Materials Science and Engineering, Northwestern University, Evanston, Illinois 60208, USA*
[2]*Sandia National Laboratories, Albuquerque, New Mexico 87185, USA*
[3]*Department of Chemical Engineering and Materials Science, University of California at Davis, Davis, California 95616, USA*

(Received 13 November 2006; published 21 March 2007)

In dendritic solidification, growth morphologies often display a pronounced sensitivity to small changes in composition. To gain insight into the origins of this phenomenon, we undertake an atomistic calculation of the magnitude and anisotropy of the crystal-melt interfacial free energy in a model alloy system featuring no atomic size mismatch and relatively ideal solution thermodynamics. By comparing the results of these calculations with predictions from recent phase-field calculations, we demonstrate that alloying gives rise to changes in free-energy anisotropies that are substantial on the scale required to induce changes in growth orientations.

DOI: 10.1103/PhysRevLett.98.125701 PACS numbers: 64.70.Dv, 05.70.Np, 68.08.−p, 81.30.Fb

In a wide class of materials, crystallization from the melt proceeds through the mechanism of dendritic growth. This process has long attracted theoretical interest as a classic example of pattern formation in a nonlinear dissipative system. For metallurgists, understanding dendrite growth is key to controlling solidification microstructures and the associated mechanical properties of cast and welded materials. A key development in the understanding of dendrite growth was the advent of microscopic solvability theory [1] which elucidates the delicate interplay between diffusive transport and capillary forces in governing the operating point of a dendrite tip. The development of a theoretical framework for understanding dendrite growth has to date focused almost exclusively on the relationship between the tip radius and velocity. From a practical point of view, an equally important, yet considerably less studied, issue is the crystalline orientation selected by the growing dendrite tip. This growth orientation affects the overall symmetry of the dendrite and is an important factor governing the morphology of solidification structures.

In most materials, dendrite tips choose high-symmetry growth directions, leading to sixfold symmetry for dendrites growing in the basal planes of hexagonal snow crystals and many hcp metals and fourfold symmetry for most cubic metals growing along $\langle 100 \rangle$. However, experimental investigations have led to a growing number of observations where alloying has been found to induce dramatic changes in solidification morphologies (e.g., [2–5]), leading to highly complex growth shapes that remain incompletely understood. In metallic alloys, such changes in solidification microstructures have important consequences for mechanical properties [3]. In the most detailed study of this phenomenon to date, Haxhimali *et al.* [5] show experimentally that over a range of Zn compositions, in commercially relevant Al-Zn alloys, the growth direction changes smoothly from $\langle 100 \rangle$ to $\langle 110 \rangle$. To interpret these results, the authors performed phase-field simulations of dendrite growth where both the fourfold (ϵ_1) and sixfold (ϵ_2) parameters characterizing anisotropy in the crystal-melt interfacial free energy (γ) were varied. The modeling study showed that in ϵ_1-ϵ_2 space, there exist regions where $\langle 100 \rangle$ and $\langle 110 \rangle$ growth are preferred, as well as an intermediate ''hyperbranched'' region where the misorientation angle, as measured from the $\langle 100 \rangle$ growth direction, varies smoothly from 0 to $\pi/4$. A key assumption in this theoretical interpretation is that alloying can lead to changes in the anisotropies of the crystal-melt interfacial free energies strong enough to induce changes in dendrite-growth direction. At present, there is no direct evidence either from experiment or simulation that this is the case. In this Letter, we present the results of atomistic calculations of anisotropic crystal-melt interfacial free energies in a model alloy system as a function of composition, demonstrating that composition-induced changes in the anisotropies can indeed be significant on the scale of the magnitudes required to induce changes in growth morphologies.

This Letter employs the capillary fluctuation method (CFM) [6] to compute composition-dependent values of γ and its anisotropy in a model alloy system from atomistic simulations. In light of the detailed experimental work presented in Ref. [5], it would be desirable to investigate the properties of the Al-Zn system directly. However, we are unaware of interatomic-potential models that accurately model alloy solid and liquid thermodynamic properties in this system, and we will thus address a more fundamental issue, that is, whether a simple model system exhibits a trend in anisotropy consistent with a change in dendrite-growth morphology. Specifically, we employ a Lennard-Jones (LJ) alloy characterized by two ratios, $\epsilon = \epsilon_{11}/\epsilon_{22}$ and $\sigma = \sigma_{11}/\sigma_{22}$, where for species i, ϵ_{ii} represents the energy of interaction, σ_{ii} is the atomic size, and the cross-species interactions are given by the Lorentz-Berthelot mixing rules as in [7]. We have chosen $\sigma = 1.0$, meaning that the two species have the same equilibrium bond lengths, $\epsilon = 0.75$, and we use the Broughton-Gilmer truncation [8] for compatibility with previous calculations of the LJ interfacial free energy [9,10]. The

temperature-composition phase diagram is computed by Monte Carlo (MC) thermodynamic integration, as described in Ref. [11], with the results shown in Fig. 1. The phase diagram is very similar to that of Cu-Ni, another system with nearly ideal solution thermodynamics, a small size mismatch, and a ratio of melting temperatures close to 0.75. Cu-Ni has been the subject of several previous phase-field-modeling studies of interface properties [12] and dendritic solidification [13,14]. This choice of model system allows us to make contact between the present results and those obtained previously in less extensive Molecular-Dynamics (MD) studies of crystal-melt interfaces in the Cu-Ni alloy [12].

Application of the CFM requires well-equilibrated solid-liquid systems. Simulation samples were created and equilibrated following a procedure very similar to that described in Ref. [11]. Specifically, samples were created by scaling the composition and atomic volume for each phase of a solid-liquid coexistence cell to the values determined from the phase diagram calculations. The cells were equilibrated using a combination of MC and MD simulations to relax the composition and stress profiles. All MD simulations in this study used the LAMMPS code [15]. For each alloy composition considered, simulation cells were set up with (100) and (110) oriented crystal-melt interfaces containing 72000 ($20 \times 20 \times 45$ fcc unit cells) and 79200 ($30 \times 20 \times 66$ fcc unit cells) atoms, respectively.

The CFM analyzes equilibrium height fluctuations to determine the stiffness of a rough crystal-melt interface and employs an expansion of the dependence of γ on interface normal in terms of cubic harmonics to determine the interfacial free energy with respect to crystalline orientation [16]. The cubic-harmonic expansion is

$$\frac{\gamma(\hat{n})}{\gamma_0} = 1 + \epsilon_1\left(\sum_i n_i^4 - \frac{3}{5}\right) + \epsilon_2\left(3\sum_i n_i^4 + 66 n_1^2 n_2^2 n_3^2 - \frac{17}{7}\right), \quad (1)$$

where $\hat{n} = (n_1, n_2, n_3)$ is the interface normal. The orientationally averaged value of γ is given by γ_0, while ϵ_1 and ϵ_2 represent the strengths of the fourfold and sixfold anisotropies, respectively. In the CFM, the values of γ_0, ϵ_1, and ϵ_2 are derived by fitting to stiffness values obtained from interface fluctuation spectra derived through equilibrium MD simulations.

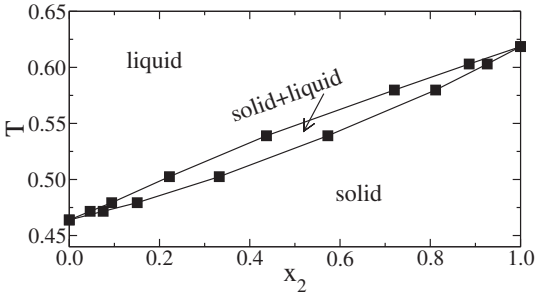

FIG. 1. Temperature-composition phase diagram calculated for the Lennard-Jones alloy characterized by $\sigma = 1.0$ and $\epsilon = 0.75$.

The methodology of the CFM has been described previously for simulation cells employing quasi-one-dimensional (1D) "ribbonlike" interface geometries (e.g., [6,17]). Here, we make use of simulation geometries containing two-dimensional (2D) interfaces in a manner similar to that employed in a recent CFM calculation of grain-boundary stiffness [18]. For 2D interfaces, the CFM exploits the following relation:

$$\langle |A(k_1, k_2)|^2 \rangle = \frac{k_B T}{a(S_{11}k_1^2 + S_{22}k_2^2 + 2S_{12}k_1k_2)}, \quad (2)$$

where $|A(k_1, k_2)|^2$ is the square of the Fourier coefficients of the 2D interface-height profiles $h(x_1, x_2)$, and $a = L_1L_2$ is the cross-sectional area of the periodic simulation cell. Although simulations with 2D interfaces require larger simulation cells (more atoms), there are advantages to using such geometries. Specifically, from two independent simulations, namely, with (100) and (110) interface normals, three independent stiffness values can be derived (see below), while three different simulations would be required to obtain the same information with quasi-1D interfaces. Also, more k-modes are accessible from a 2D interface since k-vectors have the form $2\pi(j_1/L_1, j_2/L_2)$ with either or both j_1 and j_2 nonzero. To ensure that the fluctuation amplitudes are of comparable magnitude in both the 2D and 1D geometries (for comparable signal to noise ratios), the interface area a should in Eq. (2) be similar. This gives rise to smaller periodic lengths and an associated drawback that less information is obtained for long-wavelength modes, where Eq. (2) should be most accurate, in the 2D case. In the current study, we employed 2D interface geometries in the CFM calculations because they led to a reduction in the total number of simulation cells to be equilibrated.

For 2D interfaces, the stiffness (S_{ij}) is a 2×2 tensor, and Eq. (2) can be simplified using symmetry for certain interface orientations. Specifically, for a (001) interface, with x_1 and x_2 oriented along the [100] and [010] directions of an fcc crystal, the off-diagonal terms are zero and the (nonzero) diagonal terms are equal. Similarly, for a (011) interface orientation with x_1 and x_2 along [100] and $[01\bar{1}]$, there are two independent diagonal contributions to the stiffness tensor with zero off-diagonal terms. To extract γ_0, ϵ_1, and ϵ_2, we thus employ equilibrium microcanonical MD simulations for 2D interface geometries with (100) and (110) orientations for each alloy composition considered. Fluctuation spectra were obtained from simulations lasting on the order of 10^6 time steps. Snapshots were periodically sampled, and for each, the interface-height profile $[h(x_1, x_2)]$ was determined and Fourier transformed to compute the amplitudes appearing on the left hand side of Eq. (2). After averaging over 10^3 to 10^4 configurations, interface stiffnesses were derived from least-squares fits of

TABLE I. Mean interfacial free energies γ_0, anisotropies, and anisotropy parameters (ϵ_1 and ϵ_2) for all temperatures studied. Units on γ are $(\epsilon_{22}/\sigma_{22}^2)$. Parentheses represent 95% statistical confidence levels for the last digit.

T	γ_0	$\frac{\gamma_{100}-\gamma_{110}}{2\gamma_0}$	$\frac{\gamma_{100}-\gamma_{111}}{2\gamma_0}$	ϵ_1	ϵ_2
0.464	0.267(6)	0.014(1)	0.019(2)	0.057(6)	−0.0009(5)
0.479	0.270(8)	0.012(2)	0.019(2)	0.055(7)	−0.0026(7)
0.5025	0.302(7)	0.008(2)	0.014(2)	0.043(6)	−0.0033(6)
0.539	0.327(9)	0.010(2)	0.018(2)	0.052(7)	−0.0037(6)
0.603	0.347(8)	0.010(2)	0.016(2)	0.046(6)	−0.0015(6)
0.6185	0.355(8)	0.014(1)	0.019(2)	0.057(6)	−0.0009(5)

$\langle |A(k_1, k_2)|^2 \rangle$ versus k_1^2 and k_2^2. From stiffness values thus derived, the parameters γ_0, ϵ_1, and ϵ_2 in Eq. (1) were extracted. The results are listed in Table I and plotted in Figs. 2 and 3.

The temperatures considered in the alloy calculations are indicated by the filled symbols in Fig. 1. The values of γ_0 are plotted as a function of T in the upper panel of Fig. 2, where the dotted line indicates a linear interpolation between the pure species values. The values for the pure elements obtained here agree well with previous results obtained by cleaving [10,19] and CFM [17] methods. The magnitude of the reduction in γ_0 arising from alloying species 2 with ~10% solute is comparable to that obtained in a previous CFM calculation for Ni(Cu) alloys [12].

In the ''neg-entropic'' theory of crystal-melt interfaces [20], γ is dominated by contributions from the (negative) excess entropy associated with configurational ordering of the liquid near the solid. In this theory, γ_0 is expected to vary linearly with the coexistence temperature if it is assumed that the excess entropy is independent of composition. The results in Fig. 2 show clearly this expected trend of increasing γ_0 with temperature; however, a statistically significant deviation from linearity is obtained, with γ_0 for the most concentrated compositions showing 5–10% larger values. This trend toward positive deviation from linear T dependence is consistent with phase-field-model predictions for Cu-Ni [13].

Calculated anisotropies in γ between (100), (110), and (111) orientations are plotted versus T in Fig. 2, showing that $(\gamma_{100} - \gamma_{110})/(2\gamma_0)$ is smaller than $(\gamma_{100} - \gamma_{111})/(2\gamma_0)$ at all temperatures. In other words, we compute $\gamma_{100} > \gamma_{110} > \gamma_{111}$ for all alloy compositions, a result that is consistent with previous simulation results obtained for elemental fcc metals (see Ref. [21] and references therein), as well as experimental results for fcc alloys [22]. The calculated anisotropies are small, a few percent, as expected for atomically rough interfaces.

In Fig. 3, we plot the calculated anisotropy parameters (ϵ_1 vs $-\epsilon_2$) for each of the liquidus temperatures considered. These results are overlaid on the dendrite-orientation stability diagram, mentioned above, as calculated from phase-field simulations [5]. The solid lines in the plot delineate regions where the ⟨100⟩, hyperbranched, and

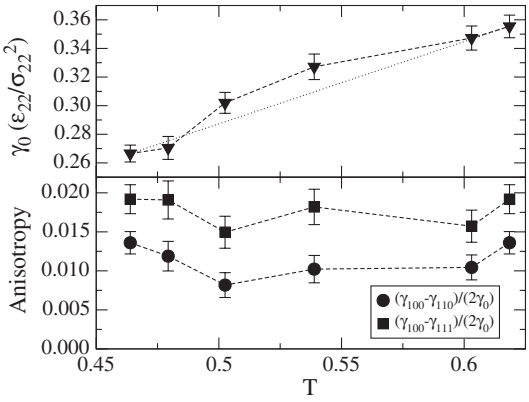

FIG. 2. γ_0 (upper panel) and free-energy anisotropies (lower panel) vs T for the LJ alloy characterized by $\epsilon = 0.75$ and $\sigma = 1.0$. The dotted line in the top figure represents a linear interpolation between the pure species values.

⟨110⟩ growth modes are preferred. The pure-element LJ results lie furthest to the left, well inside the ⟨100⟩ growth region, consistent with the most commonly observed dendrite-growth orientation for fcc metals. Starting from pure species 1 (the lowest temperature), increasing the concentration of species 2 (increasing temperature) tends to lead to an overall slight decrease in the magnitude of ϵ_1 and an increase in the magnitude of the (negative) value of ϵ_2. The effect of alloying up to concentrations of $x_2 \approx 0.5$ ($T = 0.5389$) is to move the anisotropy parameters from the ⟨100⟩ region to the boundary with hyperbranched morphologies. Further increases in concentration (temperature) return the anisotropy parameters back into the ⟨100⟩ region; this is a consequence of the use of model LJ potentials since the anisotropy parameters for the pure species ($T = 0.4639$ and 0.6185) are the same in this system. The main result of this study, i.e., the anisotropy

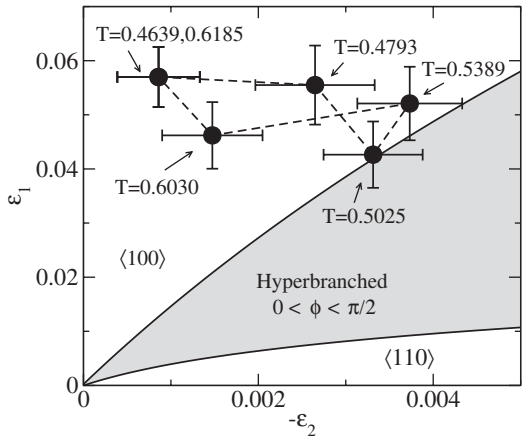

FIG. 3. Anisotropy coefficients (ϵ_1 vs $-\epsilon_2$) for the Lennard-Jones alloy with $\epsilon = 0.75$ and $\sigma = 1.0$ (definition in text) are plotted with filled symbols, where error bars denote 95% confidence intervals. The solid lines represent the borders between ⟨100⟩, hyperbranched, and ⟨110⟩ dendrites, as derived from phase-field simulations [5].

parameters determined from atomistic simulations move away from the domain of stability of ⟨100⟩ growth, suggests that this alloy would display ⟨100⟩ growth at dilute compositions but would have an enhanced tendency toward branching in concentrated alloys. These results are in qualitative correspondence with the hypothesis introduced in the interpretation of the Al-Zn experimental results by Haxhimali *et al.* [5].

The large composition dependencies of the anisotropy parameters calculated in the present work are noteworthy given the relatively simple nature of the model LJ alloy system considered. In light of these results, it is interesting to consider whether compositionally induced changes in these anisotropy parameters may be further enhanced for systems featuring more complex interatomic potentials. In the one other atomistic-simulation study of alloy crystal-melt interfacial free energies performed to date, the CFM was employed to compute γ and its associated anisotropies in Ni-Cu, employing a many-body embedded-atom potential model. The anisotropy parameters were calculated to change from $[\epsilon_1 = 0.09(6),\ \epsilon_2 = -0.011(1)]$ for pure Ni to $[\epsilon_1 = 0.072(8),\ \epsilon_2 = -0.007(1)]$ for an alloy with 10 at% Cu liquid composition. Relative to the present results, those for Ni-Cu feature substantially larger compositional changes in ϵ_1 and ϵ_2. Interestingly, however, alloying in Ni-Cu leads to a decrease in the magnitudes of both parameters, in contrast to the present results where the magnitude of ϵ_2 increases with alloying. While the Ni-Cu results reinforce the main conclusion of the Letter, namely, that alloying effects on the anisotropy of γ are large on the scale required to induce morphological changes in dendrite growth, they also suggest that the details of the interatomic potential are likely to be important in determining the overall sign and magnitude of these variations. The available atomistic results thus point to the need for further work, for a wider variety of interatomic-potential models, as a framework for clarifying the nature of the microscopic factors underlying the pronounced coupling between composition and γ anisotropies in alloys. In such work, the present results are expected to provide an important benchmark, isolating compositional from geometrical ''packing'' effects, in a system with relatively simple pairwise interactions.

In summary, we have undertaken in this Letter an atomistic calculation of the magnitude and anisotropy of the interfacial free energy in a model alloy system featuring zero atomic size mismatch and relatively ideal solution thermodynamics. The dependencies of the fourfold and sixfold anisotropy coefficients calculated in this Letter are sufficiently large to support the hypothesis that changes in the magnitudes of these parameters with composition can be strong enough to induce changes in dendrite tip orientations. The Letter thus provides insight into the often-observed strong dependence of dendrite morphologies on even small changes in alloy composition.

This research was supported by the U. S. Department of Energy, Office of Basic Energy Sciences, through Grant No. DE-FG02-06ER46282, and the Computational Materials Science Network. Sandia is a multiprogram laboratory operated by Sandia Corporation, a Lockheed Martin Company, for the DOE's National Nuclear Security Administration under Contract No. DE-AC04-94AL85000.

*Current address: Metallurgy Division, Materials Science and Engineering Laboratory, National Institute of Standards and Technology, Gaithersburg, Maryland 20889, USA

[1] J. S. Langer, in *Chance and Matter*, edited by J. Souletie, J. Vannimenus and R. Stora (North Holland, Les Houches, Amsterdam, 1987), pp. 629–711, Session XLVI.
[2] K. Pettersen, O. Lohne, and M. Ryum, Metall. Trans. A **21**, 221 (1990); S.-K. Chan, H.-H. Reimer, and M. Kahlweit, J. Cryst. Growth **32**, 303 (1976).
[3] S. Henry, P. Jarry, P.-H. Jouneau, and M. Rappaz, Metall. Mater. Trans. A **28**, 207 (1997); S. Henry, P. Jarry, and M. Rappaz, Metall. Mater. Trans. A **29**, 2807 (1998).
[4] S. Henry, T. Minghetti, and M. Rappaz, Acta Mater. **46**, 6431 (1998); A. Semoroz, Y. Durandet, and M. Rappaz, Acta Mater. **49**, 529 (2001).
[5] T. Haxhimali, A. Karma, F. Gonzales, and M. Rappaz, Nat. Mater. **5**, 660 (2006).
[6] J. J. Hoyt, M. Asta, and A. Karma, Phys. Rev. Lett. **86**, 5530 (2001).
[7] M. R. Hitchcock and C. K. Hall, J. Chem. Phys. **110**, 11433 (1999).
[8] J. Q. Broughton and G. H. Gilmer, J. Chem. Phys. **79**, 5095 (1983).
[9] J. Q. Broughton and G. H. Gilmer, J. Chem. Phys. **84**, 5749 (1986).
[10] R. L. Davidchack and B. B. Laird, J. Chem. Phys. **118**, 7651 (2003).
[11] C. A. Becker, M. Asta, J. J. Hoyt, and S. M. Foiles, J. Chem. Phys. **124**, 164708 (2006).
[12] M. Asta, J. J. Hoyt, and A. Karma, Phys. Rev. B **66**, 100101(R) (2002).
[13] G. B. McFadden and A. A. Wheeler, Proc. R. Soc. A **458**, 1129 (2002).
[14] A. A. Wheeler, W. J. Boettinger, and G. B. McFadden, Phys. Rev. A **45**, 7424 (1992); J. A. Warren and W. J. Boettinger, Acta Metall. Mater. **43**, 689 (1995).
[15] S. J. Plimpton, J. Comput. Phys. **117**, 1 (1995); www.cs.sandia.gov/~sjplimp/lammps.html.
[16] W. R. Fehlner and S. H. Vosko, Can. J. Phys. **54**, 2159 (1976).
[17] J. R. Morris and X. Song, J. Chem. Phys. **119**, 3920 (2003).
[18] S. M. Foiles and J. J. Hoyt, Acta Mater. **54**, 3351 (2006).
[19] Y. Mu and X. Song, J. Chem. Phys. **124**, 034712 (2006).
[20] F. Spaepen, Acta Metall. **23**, 729 (1975); F. Spaepen and R. B. Meyer, Scr. Metall. **10**, 257 (1976).
[21] J. J. Hoyt, M. Asta, and D. Y. Sun, Philos. Mag. **86**, 3651 (2006).
[22] S. Liu, R. E. Napolitano, and R. Trivedi, Acta Mater. **49**, 4271 (2001); R. E. Napolitano, S. Liu, and R. Trivedi, Interface Sci. **10**, 217 (2002); R. E. Napolitano and S. Liu, Phys. Rev. B **70**, 214103 (2004).